

Fermi National Accelerator Laboratory

FERMILAB-Conf-76/15-EXP
2000.000

SMALL ANGLE ELASTIC SCATTERING

J. Lach

January 1976



SMALL ANGLE ELASTIC SCATTERING*

J. Lach
Fermi National Accelerator Laboratory
Batavia, Illinois 60510

January 8, 1976

I would like to review some recent results from Fermilab on the elastic scattering of the quasi-stable charged hadrons (π^\pm , K^\pm , p^\pm). Results are now available from three Fermilab experiments, E7, E69 and E96.^{8,10} It is to a description of these three complementary experiments and a comparison of their results that I will devote my major efforts. I will also dwell on some exceedingly interesting results from a new high statistics experiment performed at SLAC.

Experiments at the ISR and at Fermilab's internal target area have taught us a good deal about elastic proton-proton scattering but it is only recently that comparable experiments using π^\pm , K^\pm and \bar{p} 's have begun to be available. Let me first briefly review the major features of the pp data.

Figures 1 and 2 display the essential features of the high energy pp data. In Fig. 1 we see the onset of the dip in the

*Invited Talk at the Triangle Conference on High Energy Particle Interactions, Bratislava, Czechoslovakia, November 1975.

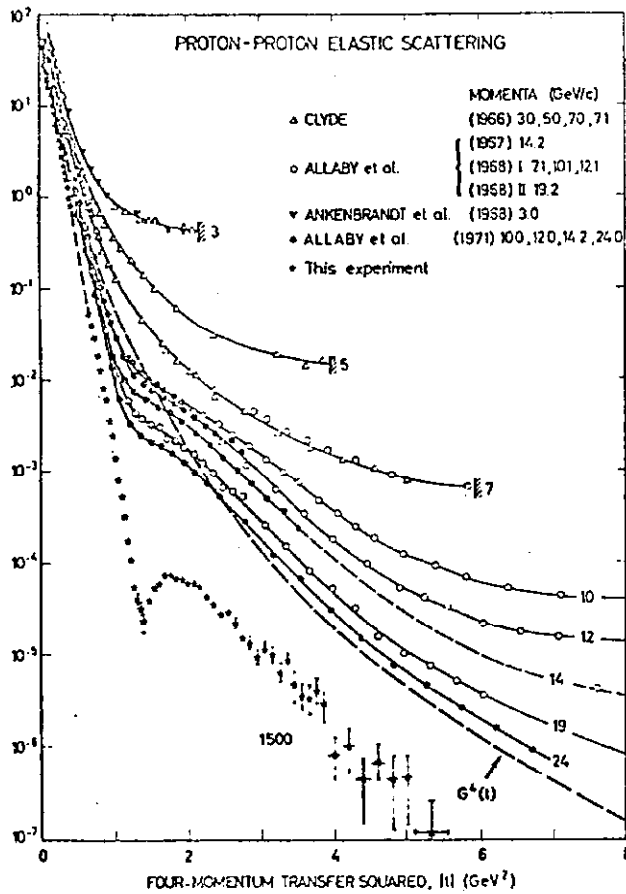


Figure 1: t distribution for pp scattering showing onset of dip at $t \sim -1.4 \text{ GeV}^2$ from Ref. 1.

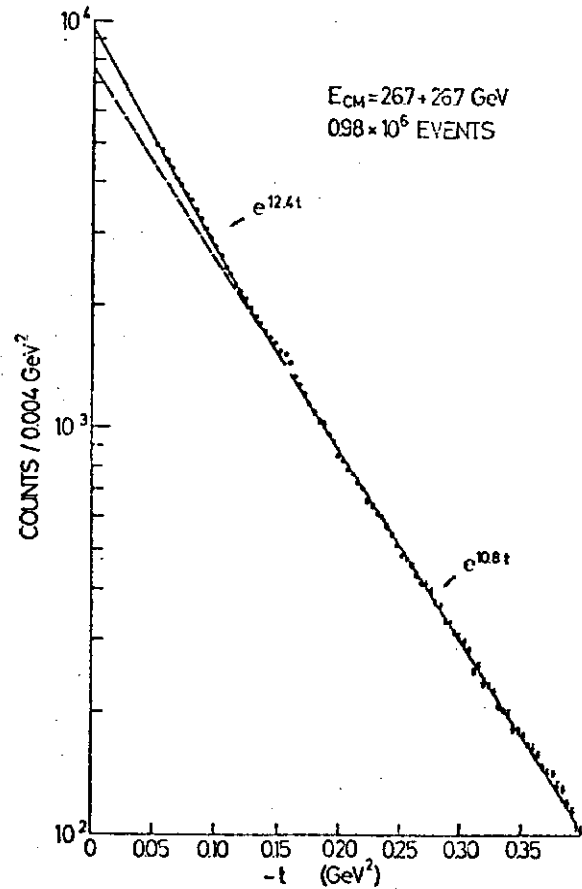


Figure 2: t distribution for pp scattering showing curvature change (break?) at $t \sim -0.14 \text{ GeV}^2$ from Ref. 2.

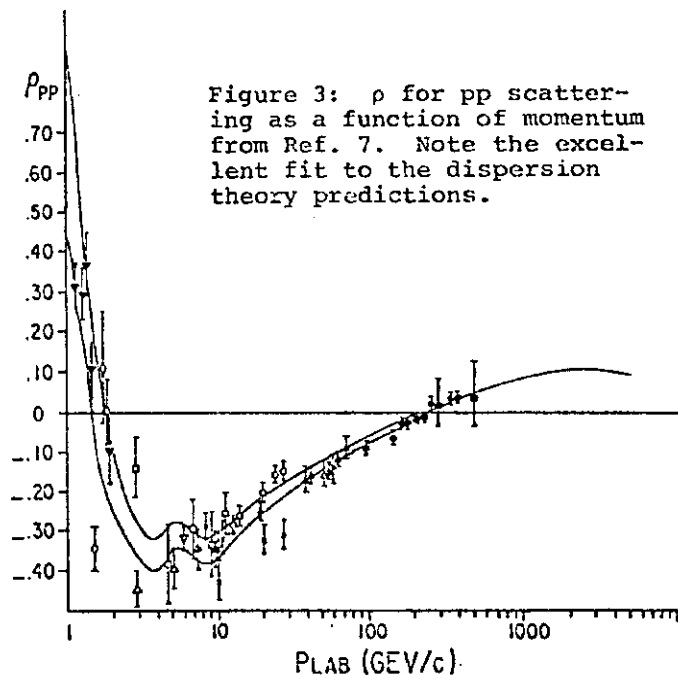
angular distribution at $t \sim -1.4 \text{ GeV}^2$. This dip appears clearly in ISR data although as seen in Fig. 1 there is a flattening of the distribution in this region even at much lower energy. Evidence of additional structure at much lower $|t|$ is seen² in Fig. 2. Again this apparent change in the slope at $t \sim -0.14 \text{ GeV}^2$ was first seen clearly in data from the ISR. However Carrigan³ in 1969, from an analysis of data from Serpukhov and lower energies conjectured that it must exist. The effect is clearly seen in

the new SLAC data⁴ at 10.4 GeV so it is not an effect unique to ISR and Fermilab energies.

Attempts to understand these features have centered about the eikonal approach pioneered by Chou and Yang⁵ and reviewed recently by Miettinen⁶. This intuitively appealing approach provides a natural explanation for the dip at -1.4 GeV^2 and requires a steepening of the slope near -0.14 GeV^2 . With new data available or soon to be available on the other particles, it will be important to make detailed comparisons with the theory.

The region at very small $|t|$ is dominated by Coulomb scattering but the transition region where both the nuclear and Coulomb terms are important allows for a measurement of the real to imaginary part of the forward scattering amplitude, $\rho = \text{Re}f(0)/\text{Im}f(0)$. Figure 3 shows the existing data for ρ_{pp} taken from a recent compilation by Hendrick and Lautrup.⁷ For comparison are shown the predictions of dispersion

relations as computed by the same authors. The good agreement with the dispersion calculation predictions not only serves as a check of such basic assumptions as analyticity and crossing symmetry but also extends our insights into the high energy behavior of total cross sections.



Of the three Fermilab experiments I will discuss, E7 and E96 are now completed, and the E7 data is in its final form.^{8,9} E69 is still completing data taking so only preliminary results on a limited data sample are available.¹⁰ Figure 4 is a comparison of the incident particle momenta and t ranges covered by these three experiments. The t range covered by E69 extends into the Coulomb region, about an order of magnitude further than indicated in the figure. Data taking at 50 and 175 GeV/c is planned but not yet completed for E69.

Each of these experiments collected data for all six particles, π^\pm , K^\pm , p^\pm , for each region shown in Fig. 4. The statistics however are considerably poorer for the minority particles in the beam, K^\pm , and \bar{p} , compared to the majority particles π^\pm and p . We can compare the statistics of these experiments if we plot as a function of t the quantity $|t| \cdot (\text{Events}/0.1 \text{ GeV}^2)$. Figure 5a, b shows this for a majority particle, π^- , and a minority particle, K^+ at 100 GeV/c; a momentum chosen because each of these experiments has collected data there. These plots tell us as a function of t , the number of events that would be available in a data bin whose width is 10% of t . For E7 and E96 the above picture of their statistics is similar at the other energies at which they ran. However for E69, since the apparatus had a fixed angular acceptance, the t bite

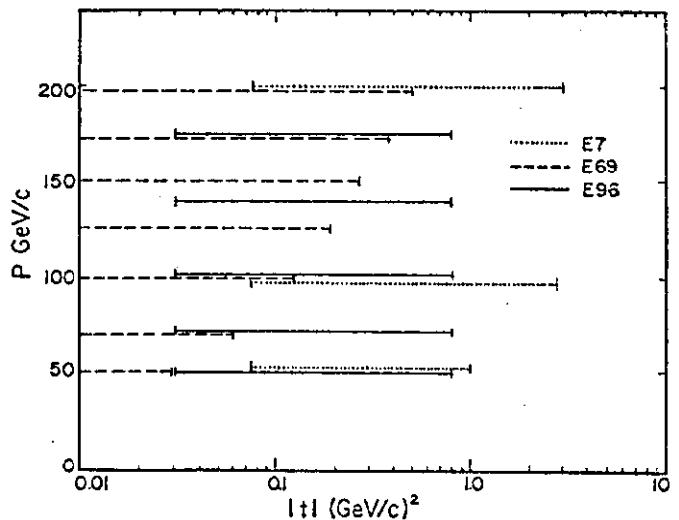


Figure 4: Nominal momenta and t ranges covered by the three Fermilab experiments.

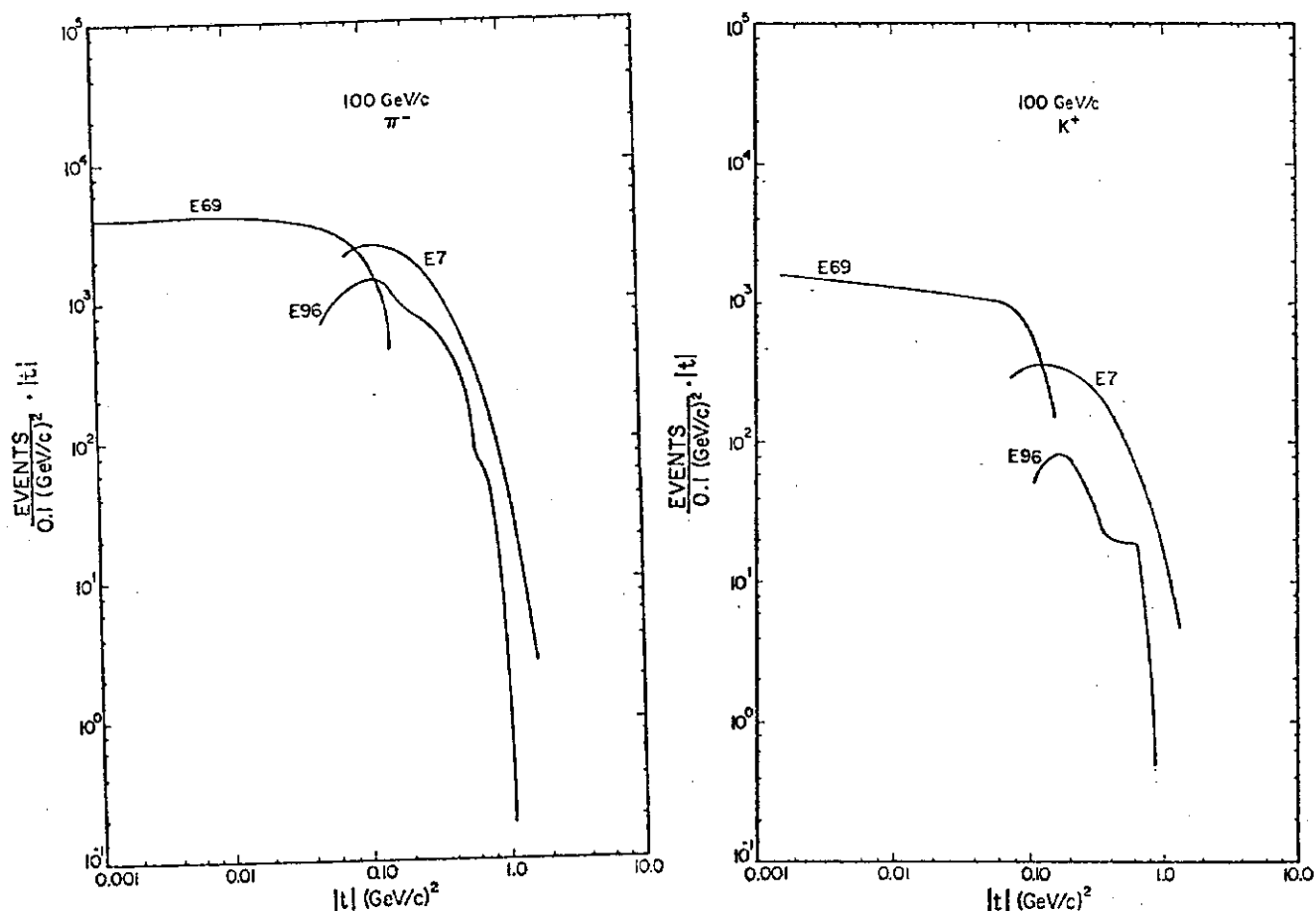


Figure 5a, b: The quantity $|t| \cdot \text{Events} / (0.1 \text{ GeV}^2)$ as a function of $|t|$ at 100 GeV/c for a majority and minority particle. This is a measure of the statistical capabilities of each experiment.

was strongly energy dependent (see Fig. 4). These experiments have significant overlap and provide us with good opportunities to make comparisons.

In Fig. 6 we also compare at 100 GeV/c the experimental resolution of each of these experiments in t . This resolution hinges on how well each of the experiments can measure angles, and although their detectors are very different, it is clear that each of them is a high resolution experiment.

A diagram of the E7 apparatus⁸ is shown in Fig. 7. It was set up in the M1 beam of the Meson laboratory and was the first of these three experiments completed. Of the three experiments,

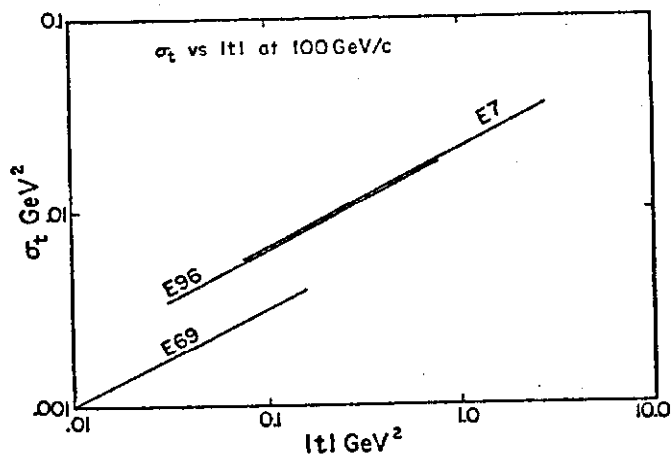


Figure 6: Experimental resolution in t , σ_t , as a function of $|t|$ at an incident momentum of 100 GeV/c for the three Fermilab experiments.

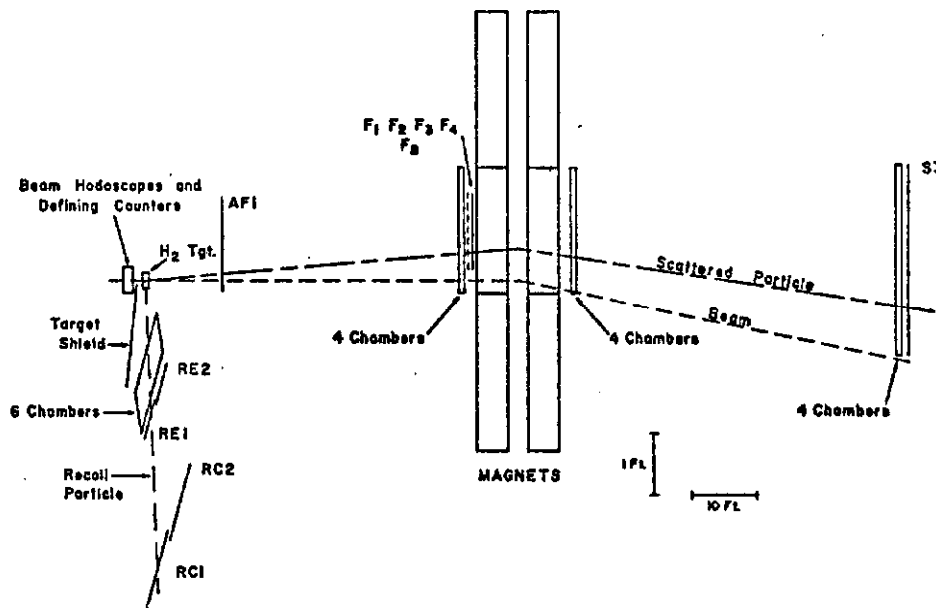


Figure 7: E7 Experimental apparatus

this is the only double arm spectrometer. The other two experiments, E69 and E96, are single arm spectrometers and hence do not detect the recoil proton. Both of the two arms were instrumented with magnetostrictive spark chambers, the forward arm in addition having two dipole magnets with an integral $B \cdot d\ell$ of 70 kG-m. This provided a momentum resolution, $\Delta p/p = \pm 1\%$ which approximately matched the $\pm 0.5\%$ momentum bite of the incident beam. The t

acceptance of the apparatus is mainly determined by the recoil arm and was quite uniform above a $|t| \approx 0.1 \text{ GeV}^2$. Below that there are losses because the recoil proton does not get out of the liquid hydrogen target. The trigger required a particle in both the forward and recoil arm thus reducing the trigger rate in this experiment compared to the other two. However, the other two experiments were able to collect data simultaneously on inelastic events, mainly target excitation, which was not possible for E7.

Of the three experiments, E7 was able to go out to the largest value of $|t|$. The acceptance extended out to $|t| \sim 7 \text{ GeV}^2$ but for protons, where they have the best statistics, the rapidly falling cross section limited $|t|$ to about 3 GeV^2 . Figure 8 shows their pp results at 100 and 200 GeV/c. The most striking feature here is the absence of the dip at $t = -1.5 \text{ GeV}^2$ in the 100 GeV/c data and its appearance at 200 GeV/c. Why this dip appears so suddenly is an interesting question. The E7 experimenters⁸ suggest

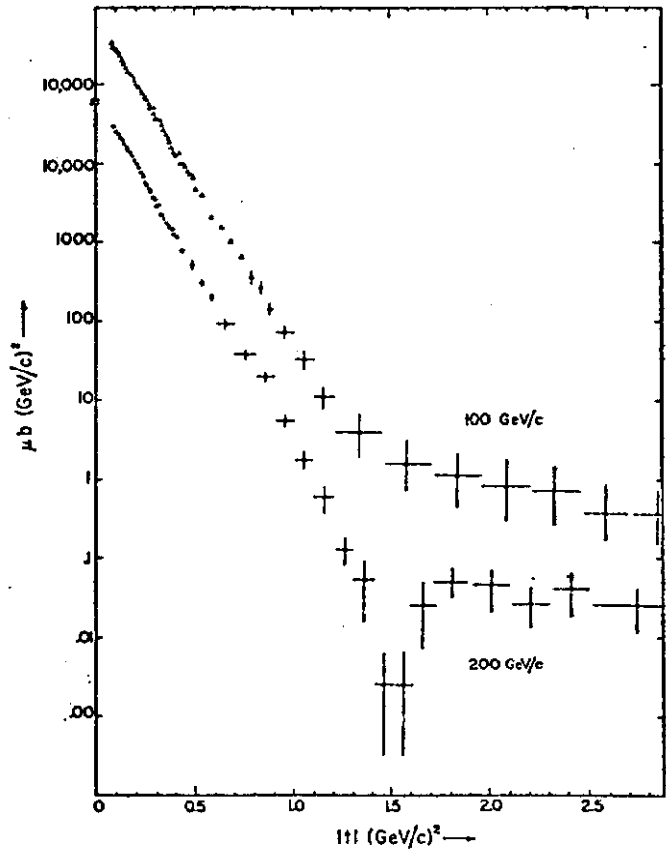


Figure 8: Differential cross section for pp scattering at 100 and 200 GeV/c showing onset of dip. Data from E7.

that it is connected with the fact that ρ goes through zero at about the energy that the dip appears. If the dip were due to the imaginary part, they argue, a significant real part could wash it out. However, if we look at Fig. 3 we note that ρ is almost as large, but of opposite sign, at the highest

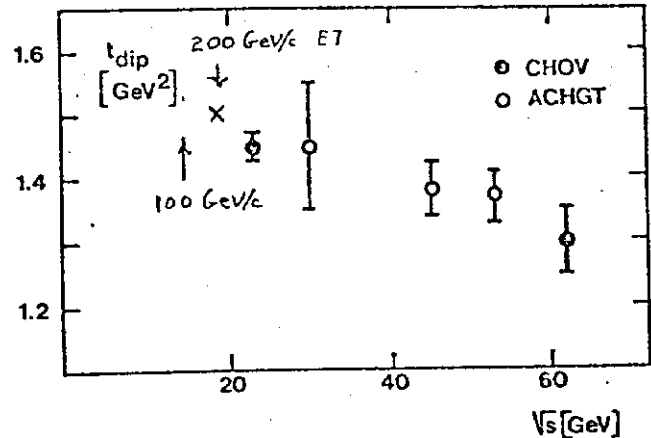


Figure 9: Position of dip in pp scattering as a function of \sqrt{s} .

ISR energies where the dip is as clearly seen (Fig. 1). It does not follow that a vanishing real part at $t = 0$ implies that it vanishes at $t = -1.4 \text{ GeV}^2$. There well may be a connection between the two phenomena but the nature of it is obscure. Figure 9 shows the change in the position of this dip as a function of \sqrt{s} . When the E7 dip position at 200 GeV/c is added to the ISR data on this figure (taken from Ref. 6), the agreement is good and makes clear the tendency of the dip to shift to smaller $|t|$ as s increases. In the simplest approach, this would indicate that the size of the scattering center is increasing with s , in agreement with the known increasing total cross section.

The E7 group has fitted their measured angular distributions to the form e^{bt+ct^2} . Some of these fitted distributions are shown in Fig. 10. The experimenters draw some interesting conclusions from these data.

- 1) The distributions for particles and their antiparticles are very similar as illustrated by Figs. 10a, b, and c.
- 2) All of the data at 50 and 100 GeV/c are well described by the form e^{bt+ct^2} .
- 3) The 200 GeV πp and pp data do not make a good fit to the above form. There appears to be a break in the data near $t = -0.4 \text{ GeV}^2$ (Figs. 10a, d, and e).
- 4) For $\pi^- p$ and pp there is a substantial increase of the slope in the small $|t|$ region as we go from 50 to 200 GeV/c. This is illustrated in figures. 10d and 10e. However beyond $|t| = 0.8 \text{ GeV}^2$ the $\pi^\pm p$ and $K^\pm p$ distributions become very similar and differ little from lower

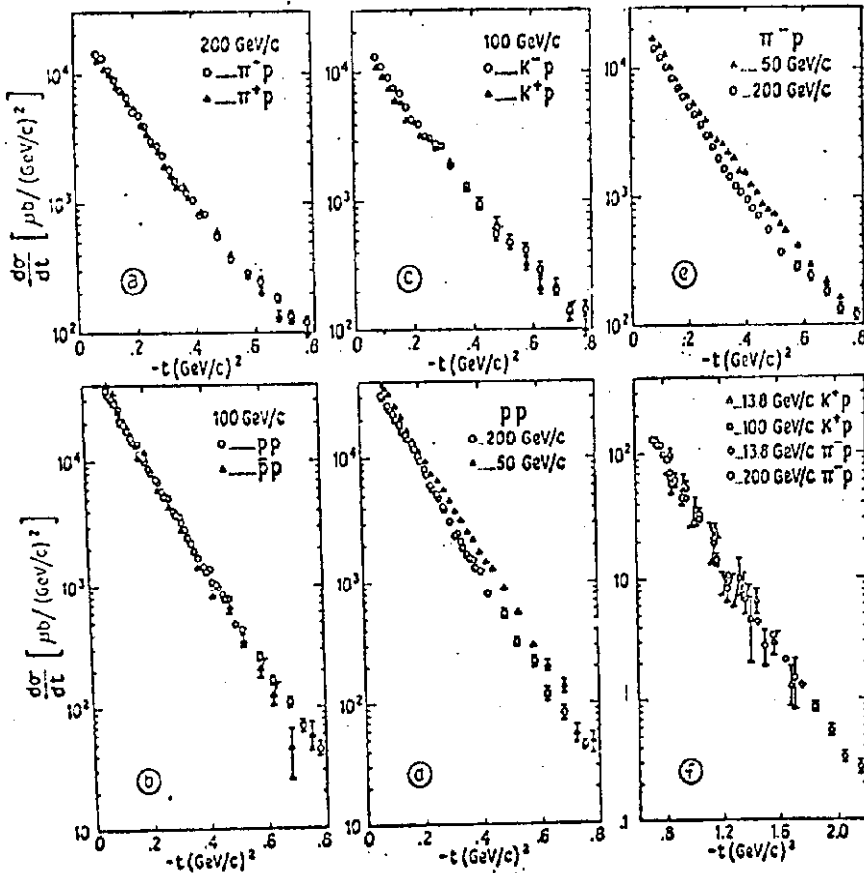


Figure 10: Measured t distributions from E7 and comparison with lower energy results.

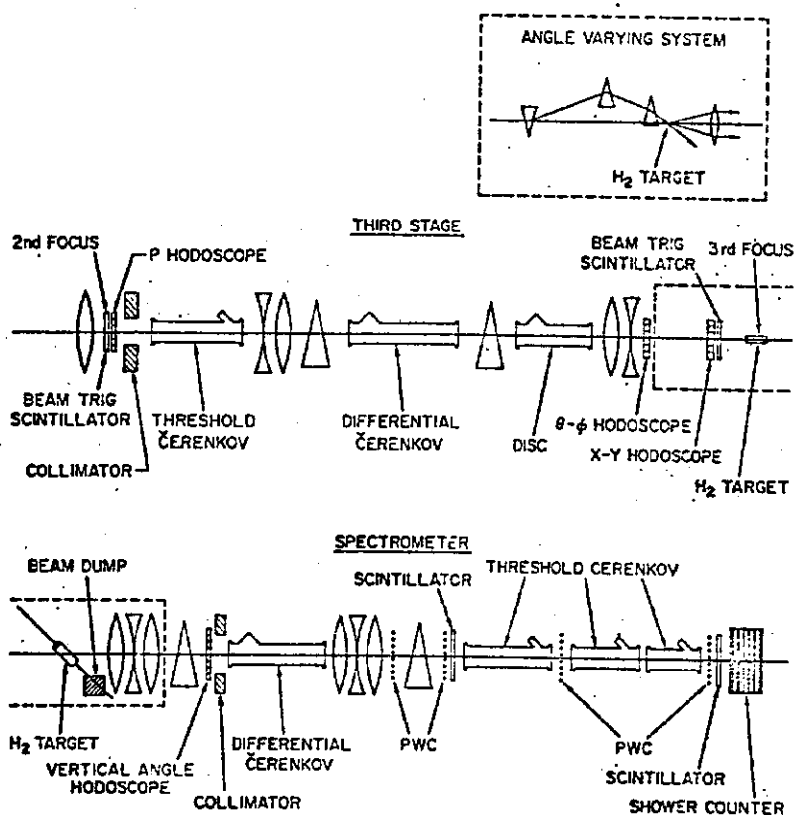
energy data. This is illustrated in Fig. 10f.

- 5) The ratio of elastic to total cross section for the mesons ($\pi^\pm p$, $K^\pm p$) is about 0.15 and for the baryons ($p^\pm p$) about 0.20 independent of the charge or particle type. This was not the case¹¹ at 40 GeV/c.

It is too early for the full significance of these results to be appreciated but they clearly raise more questions than they answer. I shall refer back to them as we make comparisons with the other experiments.

The experimental apparatus for E96 is shown in Fig. 11 and was situated in the M6E beam of the Meson laboratory. From the figure we see that this is a single arm focussing spectrometer, using scintillation counters and proportional wire chambers for detectors. The spectrometer took advantage of the excellent optics of the M6 beam line which allowed individual incident particle momenta to be tagged to $\sim 0.07\%$ and incident angles to be defined to ~ 0.1 mrad. The spectrometer acceptance was quite uniform out to a solid angle of $4.5 \mu\text{ster}$ and extended out to $7.0 \mu\text{ster}$. The direction of the incident beam impinging on the liquid hydrogen target could be varied thus allowing the spectrometer to view different production angles. For each incident momentum data was taken at a number of overlapping spectrometer settings. This accounts for the apparent structure in the E96 curves of Fig. 5. (Both E7 and E69 took their full data sample with one setting.) Particle identification was accomplished by Cerenkov detectors in the incident beam and Cerenkov counters on the spectrometer itself to identify the scattered particles.

Figure 11: The layout of the E96 spectrometer and the third stage of the M6E beam.



The apparatus included a data collection system capable of recording 200 events per accelerator pulse.

Figure 12 illustrates the excellent missing mass resolution of the E96 apparatus. Analysis of the inelastic events is not yet complete but data is available on the elastic events.⁹ Figure 13 displays the differential cross sections at 100 GeV/c. All of the E96 cross sections were well fit by an expression of the form e^{bt+ct^2} . Recall that the E7 cross sections at 50 and 100 GeV/c were also well fit by this

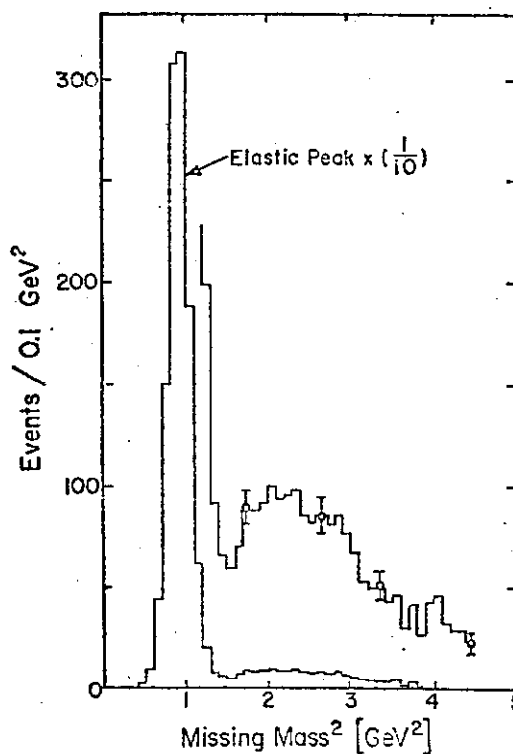


Figure 12: E96 mass resolution at 70 GeV/c incident momentum.

form but their 200 GeV/c data fitted poorly because of apparent discontinuities at $|t| \sim 0.4 \text{ GeV}^2$. The highest energy data that E96 took (Fig. 4) was 175 GeV/c so that no direct comparison with E7 can be made. It would be very nice to verify the existence of this break but unfortunately the 200 GeV/c data of E69 will probably not have sufficient statistics at large enough $|t|$ to help.

Both E7 and E96 quote values of the slope parameter b evaluated at $t = -0.2 \text{ GeV}^2$. This provides a useful consistency check for these two sets of data and I have plotted them in Fig. 14 for $\pi^- p$ and $\pi^+ p$. Note that the agreement is excellent except at the 50 GeV/c $\pi^- p$ point. The E96 point seems high compared to the trend of the other data, however it is in good agreement with the Serpukhov data.

Figure 15 displays the s dependence of the slope parameter evaluated

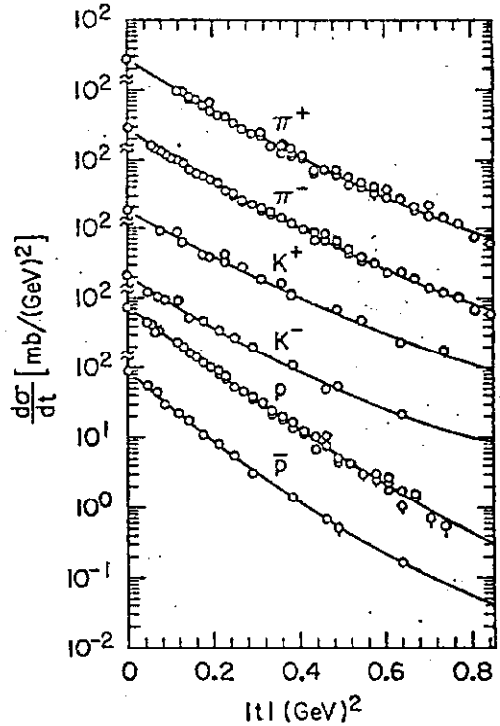


Figure 13: E96 differential cross sections at 100 GeV/c.

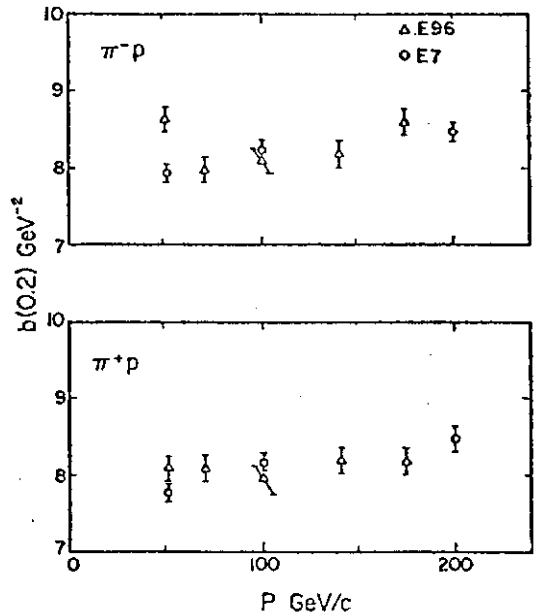


Figure 14: Slopes measured at $t = -0.2 \text{ GeV}^2$ as a function of incident momentum from E7 and E96.

at $t = -0.2$ GeV as presented by E96.⁹ In the Fermilab energy range the slopes for $\pi^\pm p$ and $K^- p$ show little energy variation. The $K^+ p$ and pp slopes still seem to be increasing whereas the $\bar{p}p$ slope is decreasing. The disagreement between E7 and E96 as to whether there is a significant change in the $\pi^- p$ slope over the Fermilab energy range results primarily because of the discrepancy between their slope measurements at 50 GeV/c mentioned in the previous paragraphs.

I will dwell at more length on E69 since less is published on it and it involves some unique instrumentation. Figure 16 shows the E69 experimental apparatus. It is a single arm spectrometer using the M6W beam of the Meson laboratory and is designed to measure the Coulomb-nuclear interference. This necessitates good angular resolution (Fig. 6) at very small $|t|$. The position and angle of the incident and scattered beam particle are determined by high precision proportional wire chambers. Two clusters of these chambers before the liquid hydrogen target measure the incident angle and two clusters behind measure the exit angle (Fig. 16). These chambers operate at a pressure of

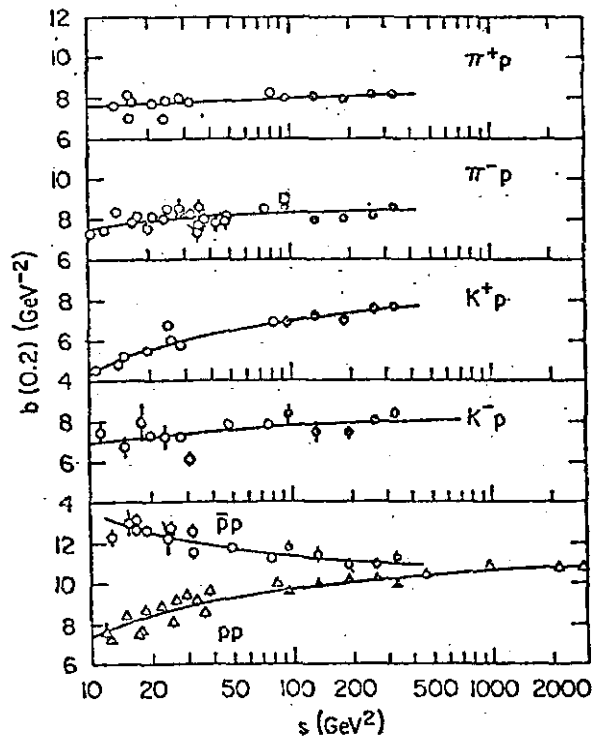
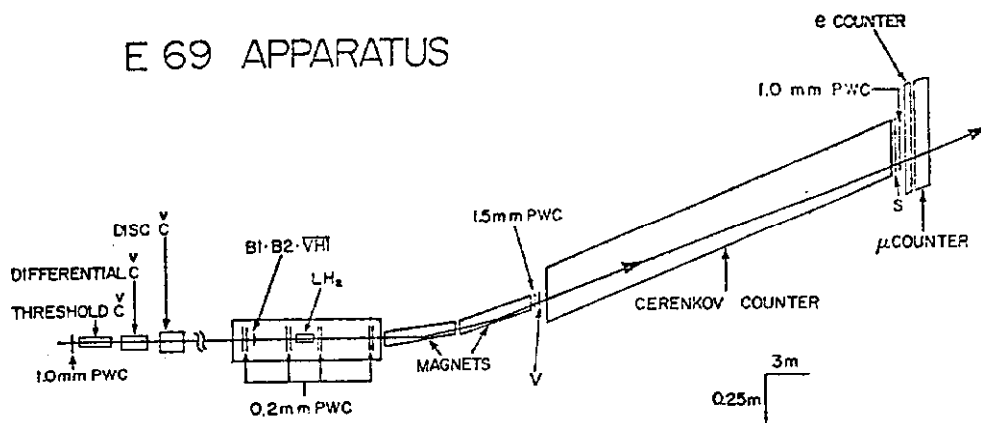


Figure 15: Energy dependence of slopes evaluated at $t = -0.2$ GeV².

E 69 APPARATUS

Figure 16: E69 experimental apparatus.



3.4 atmospheres, have an effective wire spacing of 0.2 mm and a measured spatial resolution of 70μ . To insure mechanical stability these high precision chambers which measure the scattering angle are rigidly mounted on a special concrete block (Fig. 16). As with E96, the momentum of the incident beam is measured at an upstream focus to $\Delta p/p \sim 0.07\%$. The momentum of the scattered particle is determined to almost the same precision by two main ring dipole magnets each about 6 meters long. Figure 17 shows the resolution of the E69 apparatus in p_{\parallel} and p_{\perp} . Note that at 100 GeV/c this corresponds to an angular resolution of about 0.05 mrad.

The trigger system for this experiment was complex and operated on two levels. The first level included fast logic on scintillation counters mounted on the concrete block and spatially defining the incident beam. The beam was

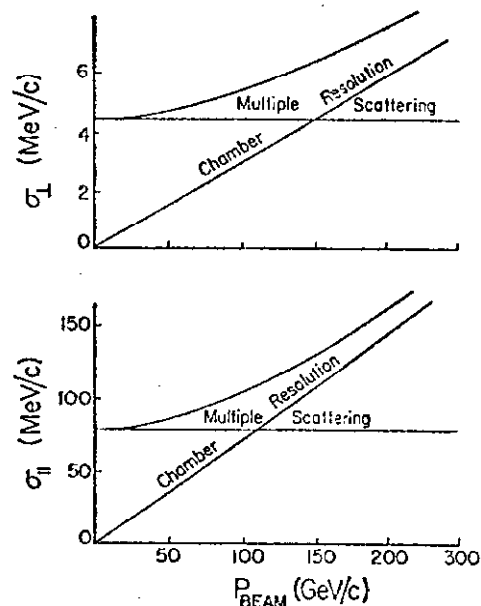
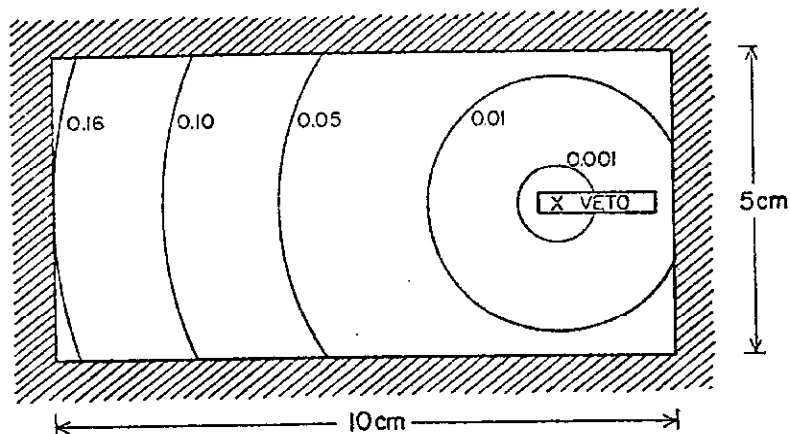


Figure 17: Resolution of the E69 apparatus in p_{\parallel} and p_{\perp}

E69 VETO PLANE GEOMETRY
100 GeV/c

Figure 18: Cross section of veto counter plane in E69. For 100 GeV/c this shows the size of the veto counter and the aperture defined by the main ring dipole magnets.



focussed not on the liquid hydrogen target but on a small scintillation counter denoted by V in Fig. 16 located downstream of the target and analyzing magnets. For an event to satisfy this first level trigger it must have been an acceptable beam particle but have missed V. The size of V was adjusted so that scatters corresponding to a value of $|t|$ less than about 10^{-3} GeV^2 would hit this counter if the beam were focussed to a point. Unfortunately even if one had perfect optics the insertion of such useful devices as Cerenkov counters and vacuum windows means that this ideal point focus is impossible in a practical beam. Hence the need for a second level of logic. Figure 18 is a cross section at V showing the size of V and the projected aperture of the main ring dipole magnets at 100 GeV/c. These are the major apertures which defined the t acceptance of the apparatus.

The second level of triggering uses the output of the high resolution proportional wire chambers to require that the beam particle be within the beam phase space (not in the beam halo) and that the beam track have scattered in the region of the target.

The condition that the incident particle be within the nominal beam phase space utilizes the correlation between position and angle from the two clusters of chambers before the target. The condition that a scattering has occurred is determined by projecting the incident particle trajectory, as determined by the upstream clusters, to the chamber cluster at the downstream end of the concrete block. If they differ by more than a predetermined amount a scattering is assumed to have occurred. Both of these tests are done simultaneously in the vertical and horizontal planes and take 3-5 μ sec. to complete.

Data on all three particle types was taken simultaneously during each beam pulse. The data collection system was capable of recording 800 events per pulse. The high data capability made it possible to sample non-interacting beam tracks, as well as events at intermediate stages of the logic on every accelerator pulse. This not only proved to be an excellent monitor of the performance of the apparatus but provided a set of beam tracks for input into the acceptance Monte Carlo calculation.

An unconventional aspect of the E69 data analysis is that it was carried out in terms of the variable $\sqrt{-t}$ (approximately equal to p_{\perp}) rather than t . This approach has the advantage that the cross section varies much less rapidly in $\sqrt{-t}$ thus making it less likely that events will spill into bins of larger $|t|$. Also since the resolution is independent of $\sqrt{-t}$, the spillage of events into adjacent bins will be independent of $\sqrt{-t}$. In Fig. 19 is shown a typical distribution in $\sqrt{-t}$ at 70 GeV/c. One sees the sharp cut

off at small values of $\sqrt{-t}$ due to the wire chamber logic requirement in the trigger. The location of $|t| = 10^{-3} \text{ GeV}^2$ has been indicated on Fig. 19.

The high resolution of the wire chambers allows the interaction vertex to be reconstructed quite accurately. Figure 20 shows the reconstructed vertex position along the beam direction for runs with the target full and empty.

One sees scattering from the hydrogen but also scattering from the chambers before and after the target. A simple cut on the position removes these events. Note that in the target empty sample one can clearly recognize scattering from the 0.005 in thick mylar windows of the liquid hydrogen flask.

As illustrated by Fig. 21, this experiment also has excellent missing mass resolution. Figure 22 illustrates a typical t distribution. Note the steep rise of the Coulomb part. These plots contain less than 10% of the available data. For their preliminary data an approximate analytic calculation of the acceptance of the apparatus was used. In this simplified computation the full t range available to the apparatus was not used and since it does not fully account for all of the apertures it does contribute

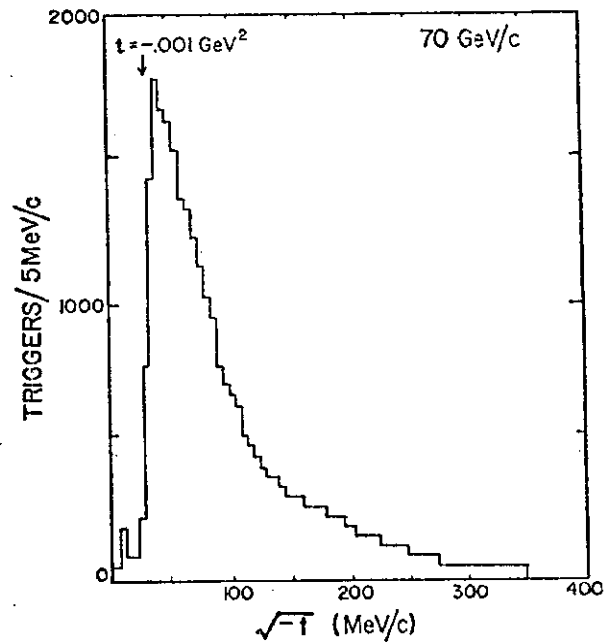


Figure 19: Event distribution in $\sqrt{-t}$ showing effect of wire chamber logic requirement that $|t| > 10^{-3} \text{ GeV}^2$.

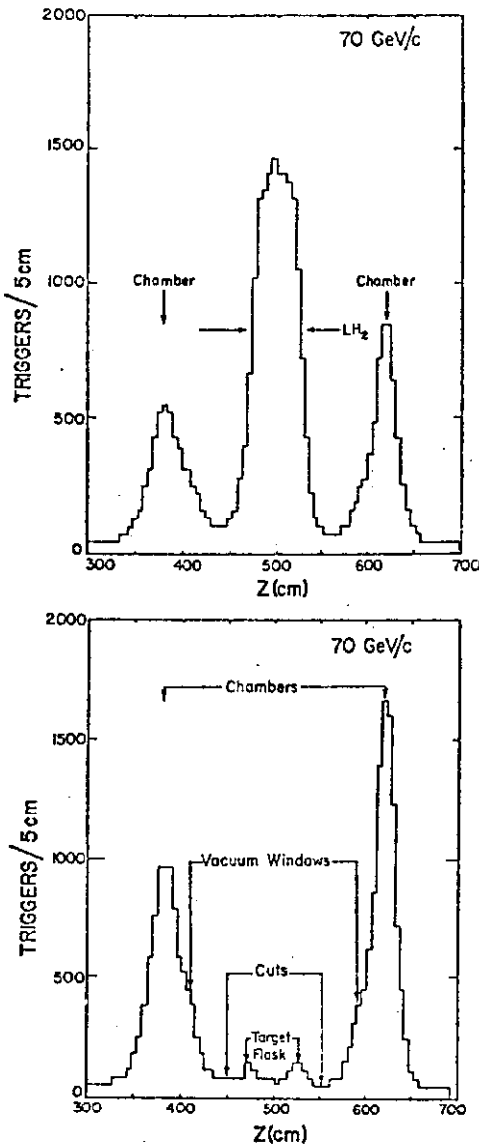


Figure 20: Reconstructed vertex position of scattered events with target full (top) and target empty (bottom).

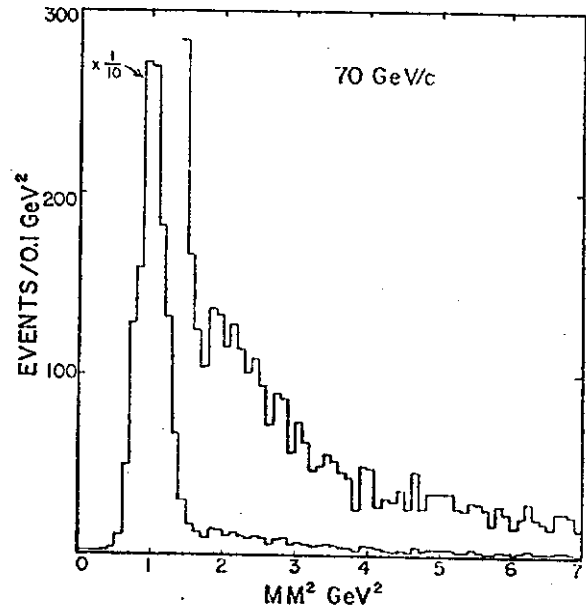


Figure 21: E69 mass resolution at 70 GeV/c incident momentum.

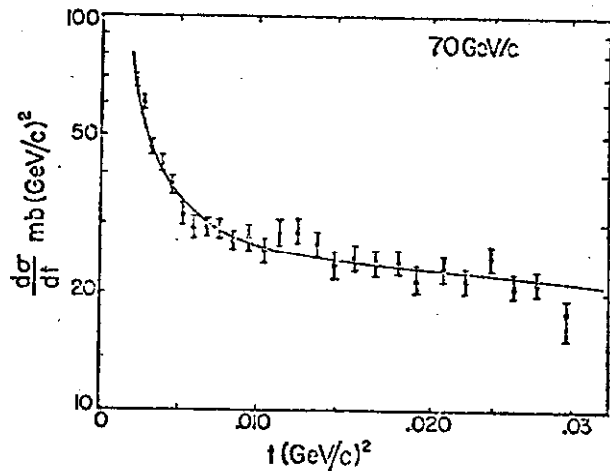


Figure 22: Typical t distribution from E69 at 70 GeV/c.

to an increased systematic error. The final analysis of the complete data sample will include a Monte-Carlo simulation of the full acceptance of the apparatus and detector resolution. Figure 23 showing the E69 acceptance in p_{\perp} at 70 GeV/c indicates the limited range that was used in the present analysis. This preliminary analysis does, however, include a first order correction for

multiple scattering and detector resolution.

The measured angular distribution of elastic events for each projectile (π^\pm , K^\pm or p^\pm) at each beam momentum is fit to the expected form of the differential cross section,

$$\frac{d\sigma^\pm}{d(-t)^{\frac{1}{2}}} = \frac{8\pi\alpha^2}{(-t)^{\frac{3}{2}}} +$$

$$\frac{(1 + \rho_\pm^2) \sigma_T^2 e^{bt} (-t)^{\frac{1}{2}}}{8\pi}$$

$$+ \frac{2 \sigma_T e^{bt/2}}{(-t)^{\frac{1}{2}}} (\rho_\pm \cos 2\delta \pm \sin 2\delta)$$

where t is the invariant four momentum transfer, α is the fine structure constant and δ is the Coulomb phase angle. The subscript + or - denotes the electric charge of the projectile. Incorporated in the fit with their errors are the recent Fermilab total cross section measurements.¹²

The results of the preliminary E69 analysis are shown in Fig. 24, along with other data and the predictions of dispersion theory.⁷ The full data sample is expected to contain 50,000 events for the minority particles (K^\pm , \bar{p}) and over 100,000 events for the majority particles (π^\pm , p) at each momentum. The results shown are from 5-10% of this sample and over a restricted t range. When

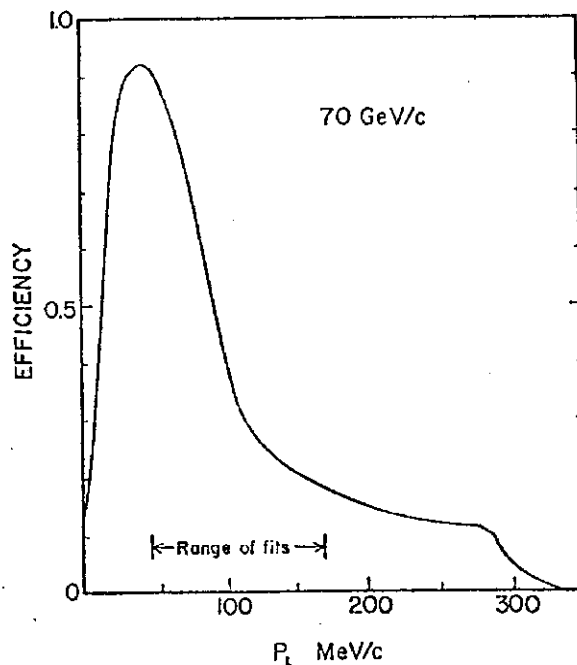


Figure 23: E69 detection efficiency as a function of p_\perp ($\sim \sqrt{-t}$) at 70 GeV/c.

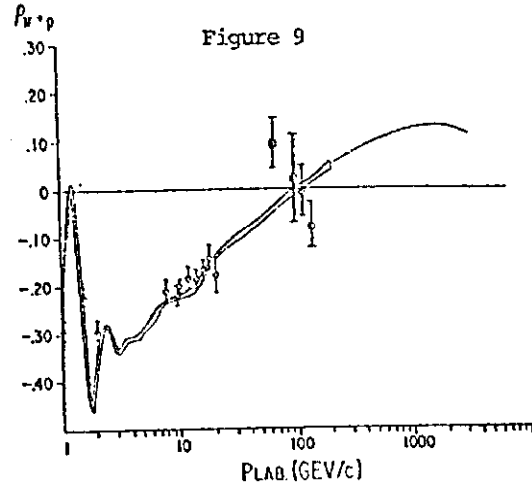
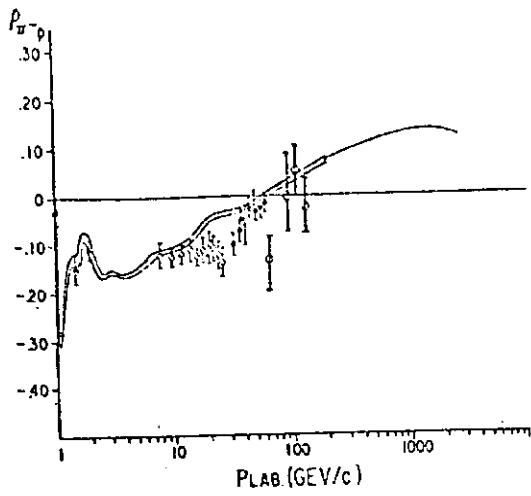


Figure 9

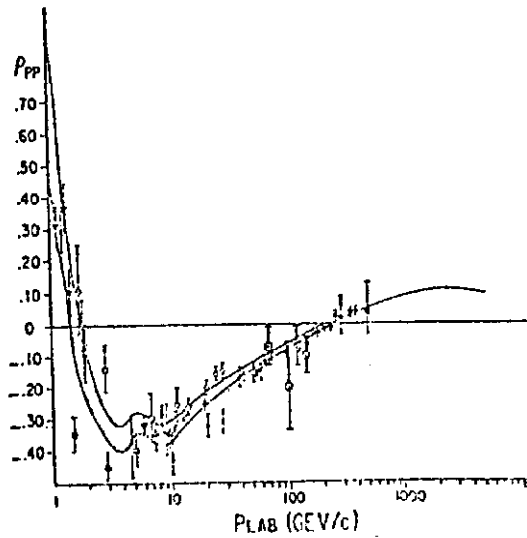
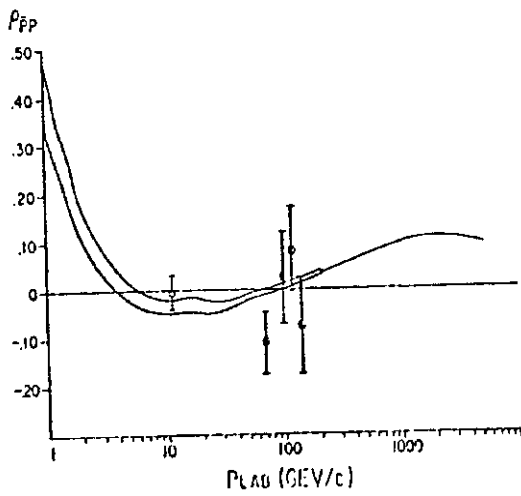
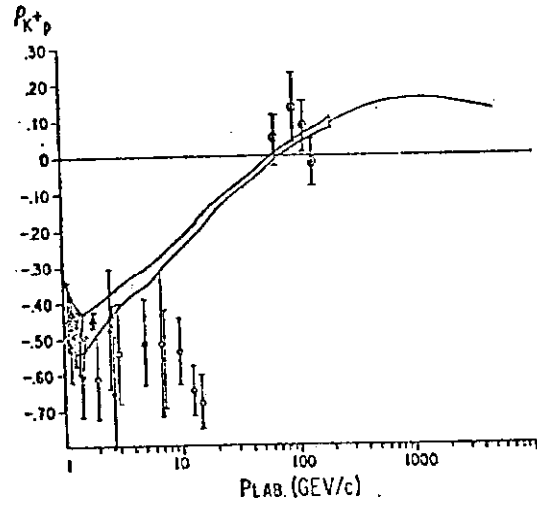
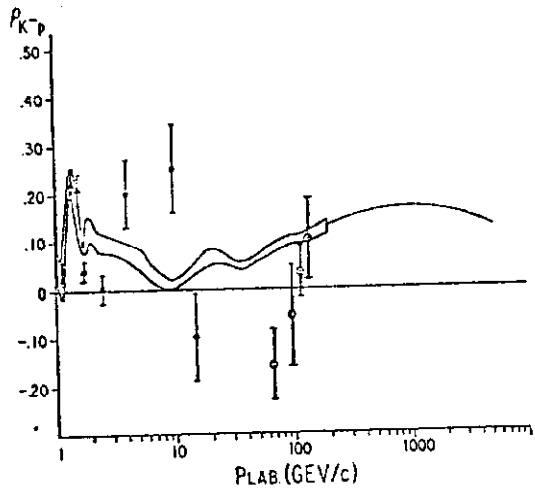


Figure 24: Preliminary E69 data on p . The E69 points are at 70, 100, 125, and 150 GeV/c.

the final data analysis is completed it is expected that the errors on ρ will be reduced to about ± 0.02 .

The data shown at 70 GeV/c has the smallest t acceptance and here in particular the results are very sensitive to the acceptance calculation. Within their present statistics and systematic uncertainties they do not feel that they are in conflict with the dispersion theory predictions.

With their large data sample E69 should be able to measure the elastic slope parameter quite accurately especially at small values of t (Fig. 5). Care was also taken not to bias the data sample against inelastic events so results should be available on the fragmentation of the target proton at small $|t|$ as a function of incident energy and particle type. Since E69 will have run a finer mesh of energies than the other experiments, it should be able to make sensitive studies of s -dependencies.

A new experiment⁴ performed at SLAC has illustrated how rich the small angle region is if explored with sufficiently high statistics. This experiment used a spectrometer instrumented with spark chambers and an rf separated beam. The spectrometer covered a t range which extended from the Coulomb region to a t of about -1 GeV^2 . However the most impressive feature is the statistics which range from 200,000 to 600,000 elastic events for each particle and energy. Such statistics are much higher than in any of the Fermilab experiments discussed here. This made it possible to

make a fit to the elastic slope in very small intervals of t , typically about 0.1 GeV^2 . Figure 25 shows the results of these fits. The striking feature is the rich structure observed in all processes. In Fig. 25 the break seen at low t in the pp data at the ISR has a counterpart in an abrupt change of curvature in pp data at 10.4 GeV . It is clear that this slope change is not a purely high energy phenomena but has been with us for a long time. It just took a very sensitive experiment to see it. The experimenters believe that their data cannot be explained by a simple diffractive picture consisting of a single Regge contribution. They can however get good quantitative agreement if a second pomeron term is included.

The new data that we have seen has been very exciting and has shown us that there is a rich structure in what was once thought of as featureless diffraction scattering. But it has raised more questions than it has provided answers. The case of pp scattering for which much more data exist than any other state, has surprised us with the rapid onset of the dip at $t = -1.4 \text{ GeV}^2$. No data exist for the other particles at a similar t region.

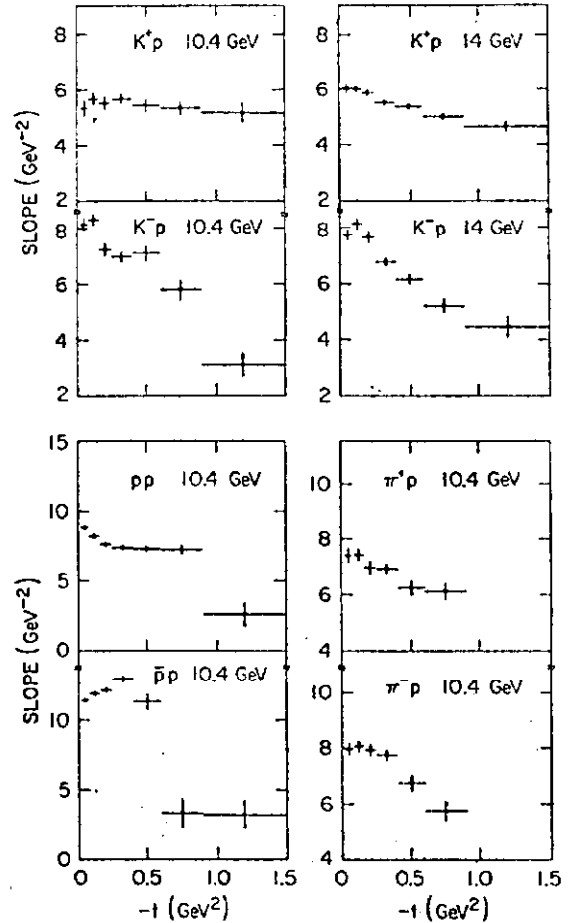


Figure 25: Elastic slope as a function of t from the SLAC result of Ref. 4.

What surprises do they hold for us? What is the nature of the curvature change (break?) at small t ? Can we make a consistent picture of the small t region including the s dependence for all the particles? The recent SLAC experiment⁴ has shown us the sensitivity that a well designed high statistics experiment can have in the small t region. There is no reason why a similar high statistics experiment could not be done at higher energies. In their simplest forms the eikonal models ignore the real parts of the scattering amplitudes. With good measurements of ρ now becoming available, what is the effect of this real part? How do we get a handle on the real part away from $t = 0$? Embedded in the Chou-Yang approach are the hadron form factors. The proton form factors are well known, the pion form factor is well measured in the time-like region but poorly known in the space-like region. No measurements exist on the kaon form factors. The experimental data in the space-like region should become much better shortly for both the kaon and pion form factors.

Can these be used to give us a consistent picture of hadron elastic scattering at high energy? How does this picture encompass diffractive excitation? A great deal of data exists, as yet not fully analyzed, on diffractive excitation of the proton by π^\pm , K^\pm and p^\pm from E96 and E69.

The next few years will be exciting ones as these high statistics and high precision counter experiments will shed light on some of our old problems and probably turn up some new surprises.

I am grateful for useful discussions with C. W. Akerlof, D. D. Yovanovitch, A. E. Brenner, G. Mikenberg and my colleagues on E69. Any errors or misconceptions, however, are solely my own responsibility.

REFERENCES

- ¹A. Bohm et al., Phys. Letters 49B, 491 (1974).
- ²G. Barbiellini et al., Phys. Letters 39B, 663 (1972).
- ³R. A. Carrigan, Jr., Phys. Rev. Letters 24, 168 (1970).
- ⁴R. K. Carnegie et al., Phys. Letters 59B, 308 (1975), and R. K. Carnegie et al., Phys. Letters 59B, 313 (1975).
- ⁵T. T. Chou and C. N. Yang, Phys. Rev. 170, 1591 (1968).
- ⁶H. I. Miettinen CERN Ref. TH. 1906, Aug. 1964.
- ⁷R. E. Hendrick and B. Lautrup, Phys. Rev. D11, 529 (1975).
- ⁸C. W. Akerlof et al., Phys. Letters 59B, 197 (1975) and C. W. Akerlof et al., University of Michigan UM HE75-21.
- ⁹Fermilab Single Arm Spectrometer Group, Fermilab-PUB-75/48 EXP.
- ¹⁰C. Ankenbrandt et al., FERMILAB-CONF-75/61-EXP.
- ¹¹A. N. Diddens, Rapporteur's talk at XVII International Conference on High Energy Physics. London 1974.
- ¹²A. S. Carroll et al., Fermilab-PUB-75/51-EXP 7100.104.